Electronic Supplementary Material (ESI) for Journal of Materials Chemistry C.

Supplementary Information: Photoluminescence engineering with nanoantenna phosphors

Shunsuke Murai,*,† Feifei Zhang,‡ Koki Aichi,† and Katsuhisa Tanaka†

†*Department of Material Chemistry, Graduate School of Engineering, Kyoto University, Nishikyo-ku, Kyoto 6158510, Japan*

‡*State Key Laboratory of Optical Technologies on Nano-Fabrication and Micro-Engineering, Institute of Optics and Electronics, Chinese Academy of Sciences, PO Box 350, Chengdu, 610209, China*

E-mail: murai@dipole7.kuic.kyoto-u.ac.jp

Contents

1 Simulation for single TiO_2 nanoparticle

For the design of the nanoantenna phosphor, we simulated the forward and backward scattering intensities by the single TiO_2 nanoparticle on the phosphor plate. The lightsource (λ= 550 nm, representing the PL wavelength of the phosphor) was embedded in the phosphor plate with the refractive index of 1.84. The forward scattering into the air side and backward scattering into the plate side from the disk-shaped TiO_2 (refractive index = 2.3) were simulated (see Fig. S1(a) for the model geometry). We varied the height and radius of the TiO_2 nanoparticle and the scattering efficiency, i.e., the scattering cross section divided by the geometric cross section, was plotted in a colormap. For the forward scattering (Fig. S1(b)), taller particles with reasonably large radius possess large scattering efficiency. This result shows that a certain size is required to obtain notable scattering, because it requires a certain size to trap the light inside the nanoparticle. This is in sharp contrast to the metal nanoparticle, where the resonance occurs carrier displacement at the surface thus the size of nanoparticle can be much less than the wavelength. For the backward scattering (Fig. S1(c)), the general trend is similar to the forward case, but the distribution is slightly different. It is also noticed that the maximum value (2.05) is less than that for the forward scattering (7.72). We divided the cross section of the forward scattering by that of the backward scattering (Fig. S1(d)). Because of the general tendency of larger forward scattering, the value is more than unity in large part of the colormap. Again, the larger value is generally obtained for the larger nanoparticle, and some sweet spots exist showing the high values.

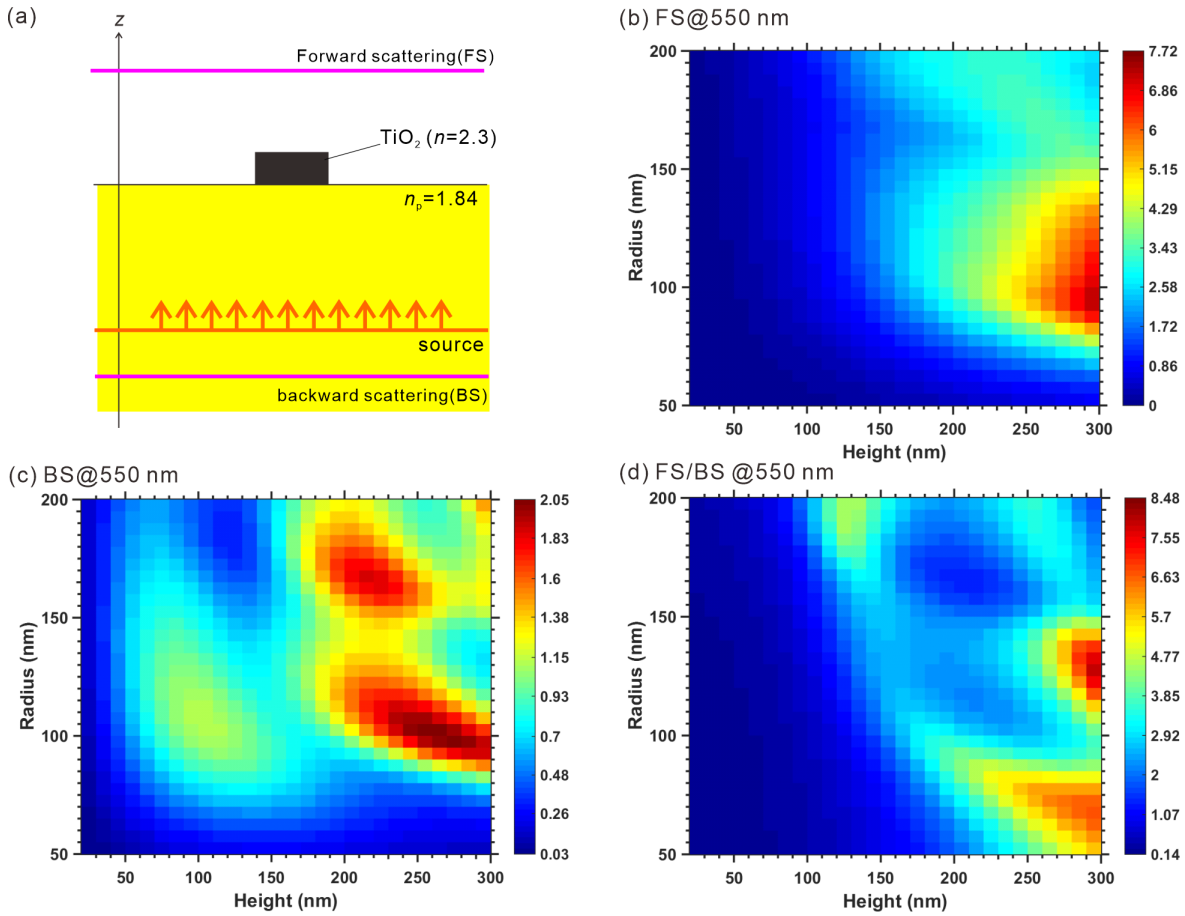

Figure S 1: (a) Simulation model for the forward and backward scattering from the single TiO_2 nanoparticle on the phosphor plate. (b,c) Efficiency of forward (b) and backward (c) scattering, defined by the scattering cross section divided by the geometrical cross section, as functions of nanoparticle height and radius. (d) Forward to backward scattering ratio, i.e., (b) divided by (c).

2 Spectral relation between extinction and emission

2.1 Effect of distributed Bragg reflector (DBR)

PL enhancement by the nanoantenna into forward direction is closely related to the extinction spectra (see the extinction spectra as a function of θ_{in} for the nanoantenna phosphor without and with a distributed Bragg reflector (DBR) in Figs. S2(a) and (b), respectively). The dotted lines represent the Rayleigh anomalies. The colormap for the nanoantenna phosphor without DBR shows a clear change in colors at the edges of the Rayleigh anomalies. A broad and dispersion-less peak appears at $\lambda \sim 520$ nm and $\theta \sim 0°$, which is a local Mie resonance at each nanoparticle. For the extinction with DBR, the extinction edge around the Rayleigh anomaly is less notable due to the effect of reflection by DBR. The comparison between the extinction and the emission at normal direction, in Fig. S2(c), is suggestive for the origin of PL enhancement. For the extinction, a broad local Mie resonance appears at $\lambda \sim 520$ nm for both samples. For the nanoantenna with DBR, an additional resonance appears at $\lambda \sim 630$ nm due to DBR reflection. PL enhancement spectra follow the features appearing in extinction, showing a local maximum at $\lambda \sim 520$ nm for both samples, and additional peak at $\lambda \sim 630$ nm for the nanoantenna with DBR. The enhancement value of 12 times is the highest among the values for TiO_2 nanoantenna on the YAG:Ce plate in previous works,[1–4] and larger than the Al nanoantennas on the YAG:Ce plate by more than two times.[5]

2.2 Comparison with simulation

We simulated the extinction of the nanoantenna phosphor using a FDTD method (Lumerical). The TiO_2 nanoparticle was modeled as a disk with radius and height being set to 200 and 250 nm, respectively, and with a dispersion-less refractive index of 2.3. The disks were arranged on the substrate with the dispersion-less refractive index of 1.84, and the periodic boundary condition was applied to simulate the array. The diffractive features appeared in the experimental map are reproduced by the simulation (Fig.S3). The discrepancy of ex-

tinction intensity is ascribed to the refractive index of the substrate used for the simulation: The real YAG:Ce plate has absorption at the blue region in the visible spectrum.

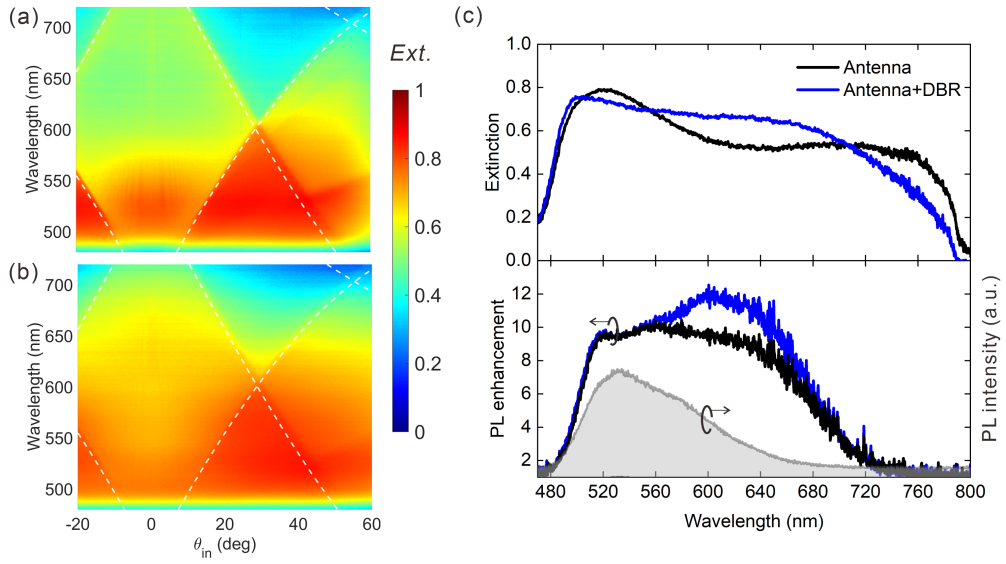

Figure S 2: Extinction spectra as a function of θ_{in} for the nanoantenna phosphor (plate thickess =105 μm) (a) without and (b) with the DBR. (c) (upper panel) Cut of the extinction map at $\theta_{\text{in}} = 0°$. (lower) PL enhancement at $\theta_{\text{em}} = 0°$. Typical PL spectrum for the flat plate is also plotted as a grey area.

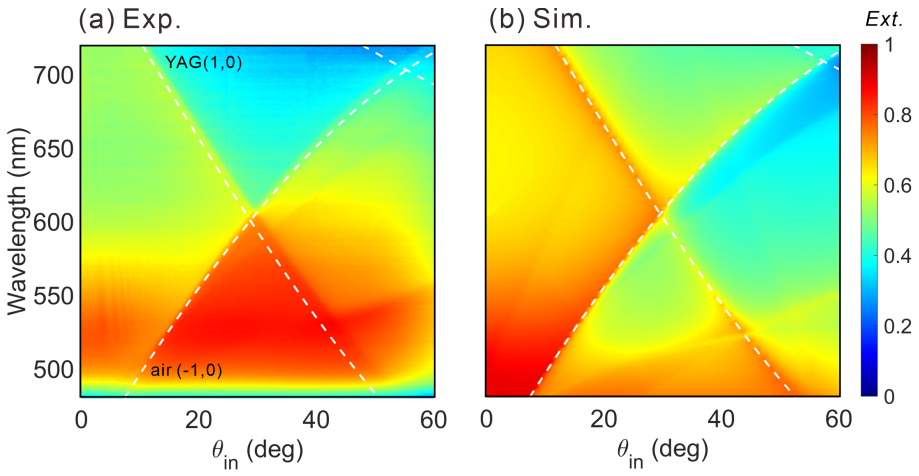

Figure S 3: Extinction spectra as a function of θ_{in} for the nanoantenna phosphor, (a) experimentally obtained for the plate thickess =105 μm and (b) obtained via FDTD simulation.

3 Measurements using integrating sphere

3.1 Absorptance, Transmittance, Reflectance and Conversion efficiency

In order to understand the flow of PL in nanoantenna phosphors comprehensively, we have conducted the measurements under five configurations: As shown schematically in Figs. S4(a)-(e), the spectra are recorded for the sphere without the plate (a), with the plate and the laser beam hitting first the sphere wall (b), with the plate and the laser beam hitting directly the plate (c), with the plate on the front port (d), and on the back port (e). From the measured spectra, we extract the following quantities: the laser beam intensity (L_{a}, L_{b}, L_{c}, and L_{d} for (a), (b), (c), and (d), respectively) and the total PL intensity integrated over the corresponding emission wavelengths (P_{b}, P_{c}, P_{d}, and P_{e} for (b), (c), (d) and (e), respectively). When a fraction μ of the laser beam scattered from the sphere wall is absorbed by the plate, L_{b} and L_{c} are given by[6]

$$L_{\mathrm{b}} = (1-\mu)L_{\mathrm{a}}, \tag{1}$$

and

$$L_{\mathrm{c}} = (1-A)(1-\mu)L_{\mathrm{a}}, \tag{2}$$

where A is the absorptance by the plate at the excitation wavelength. This absorptance can be written from Eqs.1 and 2 as

$$A = 1 - \frac{L_{\mathrm{c}}}{L_{\mathrm{b}}}, \tag{3}$$

transmittance T is the ratio of L_{a} and L_{d},

$$T = \frac{L_{\mathrm{d}}}{L_{\mathrm{a}}}, \tag{4}$$

and reflectance R is:

$$R = 1 - A - T. \tag{5}$$

The total PL is given by the absorptance of laser beam multiplied by a conversion efficiency η_c, and can be expressed as

$$\eta_c L_a A = P_c - (1 - A)P_b, \tag{6}$$

and thus

$$\eta_c = \frac{P_c - (1 - A)P_b}{L_a A}. \tag{7}$$

3.2 $\mathbf{P}_{total}$, $\mathbf{P}_{for}$, $\mathbf{P}_{side}$, and $\mathbf{P}_{bak}$.

We extracted the total PL, P_{tot}, by subtracting the effect of indirect excitation from the direct

$$P_{tot} = P_c - (1 - A)P_b. \tag{8}$$

The forward P_{for} and backward P_{bak} PLs are as follows:

$$P_{for} = P_d, \tag{9}$$

$$P_{bak} = P_e. \tag{10}$$

Because P_d and P_e are measured outside of the sphere, the indirect excitation is negligible for them. Here the value of P_{bak} is corrected by the data for the flat plate, assuming that the P_{for}=P_{bak} for the flat plate due to the out-of-plane symmetry. The side emission, P_{side} is then

$$P_{side} = P_{tot} - P_{for} - P_{bak}. \tag{11}$$

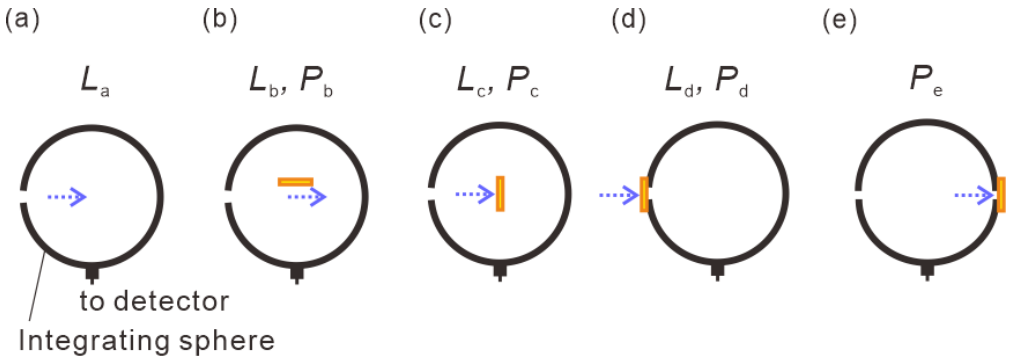

Figure S 4: Sketch of the five configurations for optical characterization. The spectra are recorded for the sphere (a) without the sample, (b) with the sample and the laser beam hitting first the sphere wall, and (c) with the sample and the laser beam hitting the sample. (d) The measurement with the sample on the front port is for the transmission of the blue laser and the forward emission.(e) The measurement with the sample on the back port is for the back emission.

4 Analytical model

4.1 Flat YAG:Ce plate with and without DBR

We calculated A, R and T using n_{p}, T_{p} and l_{a} (absorption length of the blue laser) as follows:

$$R = (\frac{n_{\mathrm{p}} - 1}{n_{\mathrm{p}} + 1})^2. \tag{12}$$

$$T(T_{\mathrm{p}}) = [1 - (\frac{n_{\mathrm{p}} - 1}{n_{\mathrm{p}} + 1})^2]e^{(-T_{\mathrm{p}}/l_{\mathrm{a}})}. \tag{13}$$

$$A(T_{\mathrm{p}}) = [1 - (\frac{n_{\mathrm{p}} - 1}{n_{\mathrm{p}} + 1})^2](1 - e^{(-T_{\mathrm{p}}/l_{\mathrm{a}})}). \tag{14}$$

We fit the model to the experimental data, with l_{a} being the single fitting parameter. The result in Fig. S5(a), top panel shows that the correspondence between the calculation (solid line) and experimental (circles) is perfect for the flat plate using l_{a}= 46 μm. We then calculated the PL distribution P_{tot}, P_{for}, P_{bak}, and P_{side} as a function of plate thickness with l_{a}= 46 μm (Fig. S5(a), bottom panel), following the formalism in the main text. The calculation reproduces the experimental tendency.

For the flat plate with DBR, we can reproduce A, R and T of the experimental data with l_{a}= 46 μm (Fig. S4(b), top panel). For the blue excitation light, the presence of DBR does not change R. For the PL, we introduce a reflection term, R_{e}. Then the forward radiation becomes

$$P_{\mathrm{for}}(T_{\mathrm{p}}) = (1 + R_{\mathrm{e}})P_{\mathrm{tot}}(T_{\mathrm{p}})\frac{\int_0^{\theta_{\mathrm{c}}} sin\theta d\theta}{2}. \tag{15}$$

and the backward radiation becomes

$$P_{\mathrm{bak}}(T_{\mathrm{p}}) = (1 - R_{\mathrm{e}})P_{\mathrm{tot}}(T_{\mathrm{p}})\frac{\int_0^{\theta_{\mathrm{c}}} sin\theta d\theta}{2}. \tag{16}$$

We fit the model to the experimental data with R_{e} being the single fitting parameter. The agreement between the calculation and the experimental is reasonable with R_{e}= 0.15 (Fig.

S5(b), bottom panel).

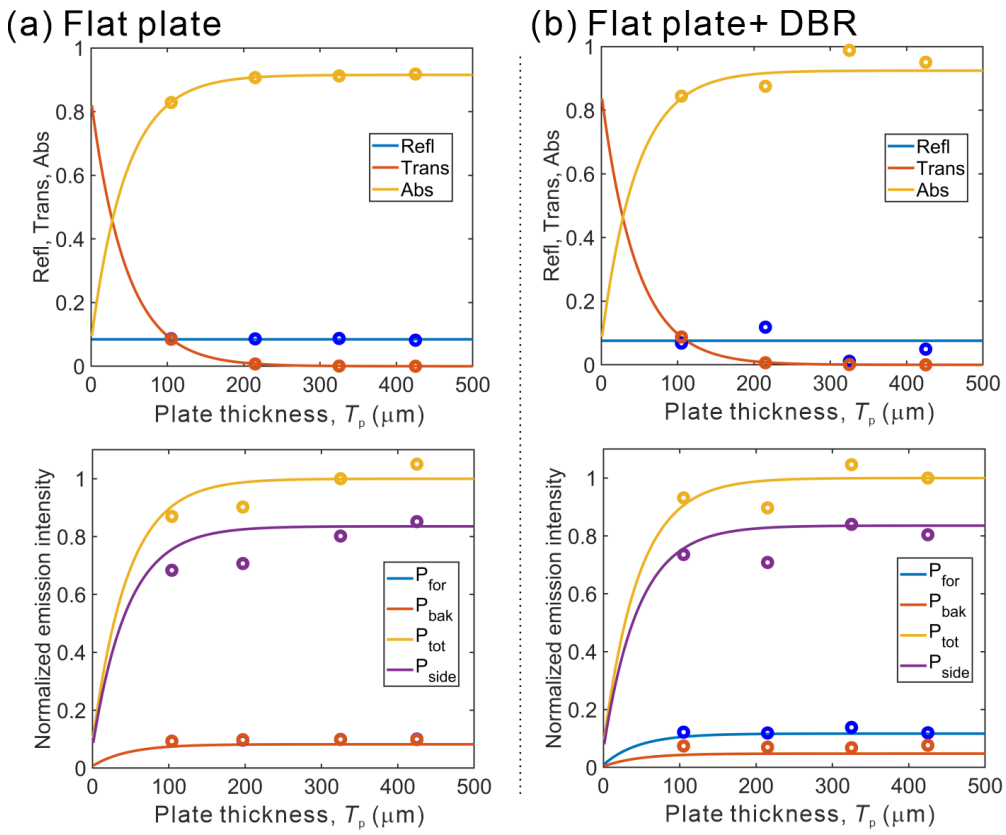

Figure S 5: (Top panel) Absorptance A, Reflectance R, and Transmittance T of the excitation blue laser (λ= 460 nm) for the flat YAG:Ce plate (a) with and (b) without the DBR as a function of the plate thickness. (Bottom panel) PL distribution $P_{\rm tot}$, $P_{\rm for}$, $P_{\rm bak}$, and $P_{\rm side}$ calculated using the analytical model(solid lines) and the experimental data (dots). In the bottom panel of (a), $P_{\rm for}$ is overlapped with $P_{\rm bak}$. In the bottom panels, the experimental values in (a) and (b) are normalized to $P_{\rm tot}(T_{\rm p}$= 325 μm) and $P_{\rm tot}(T_{\rm p}$= 425 μm), while the calculated values are normalized to $P_{\rm tot}(T_{\rm p} = \infty)$ for both (a) and (b).

4.2 Nanoantenna phosphor with and without DBR

For the nanoantenna phosphor, eq.15 becomes

$$P_{\mathrm{for}}(T_{\mathrm{p}}) = (1 + R_{\mathrm{e}}) \int_0^{T_p} p_{\mathrm{for}}(z) dz, \tag{17}$$

while P_{bak} is the same as eq.16. Using the l_{a}= 46 μm and R_{e}= 0.15, the experimental data are reproduced (see Figs. S6(a) and (b) for the nanophosphor without and with DBR, respectively).

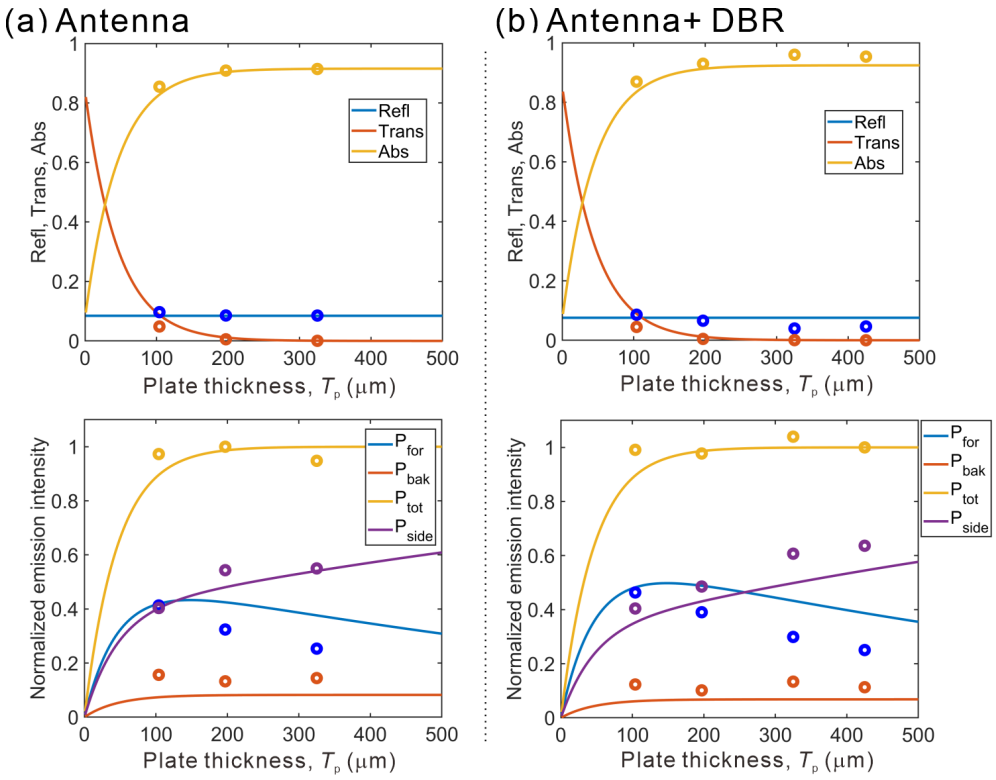

Figure S 6: (Top panel) Absorptance A, Reflectance R, and Transmittance T of the excitation blue laser (λ= 460 nm) for the nanoantenna phosphor (a) with and (b) without the DBR as a function of the plate thickness. (Bottom panel) PL distribution P_{tot}, P_{for}, P_{bak}, and P_{side} calculated using the analytical model(solid lines) and the experimental data (dots). In the bottom panels, the experimental values in (a) and (b) are normalized to $P_{\mathrm{tot}}(T_{\mathrm{p}} = 197\ \mu\mathrm{m})$ and $P_{\mathrm{tot}}(T_{\mathrm{p}} = 425\ \mu\mathrm{m})$, while the calculated values are normalized to $P_{\mathrm{tot}}(T_{\mathrm{p}} = \infty)$ for both (a) and (b).

4.3 Effect of the antenna radius and the reflection term

We examine the effect of antenna radius (R_a) on P_{for} by using the analytical model. We calculated for the plate thickness = 105 μm the distribution ratio of P_{for}, P_{bak}, and P_{side} as a function of R_a with different R_e of 0.0, 0.5 and 1.0 (Fig. S7). When R_e is 0.0, P_{for} increases as the increase of R_a and it saturates around 0.5, because half of the PL is radiated into the opposite side of the antenna. When R_e is 1.0, P_{bak} is suppressed and all the PL is radiated into forward direction when R_a is large enough.

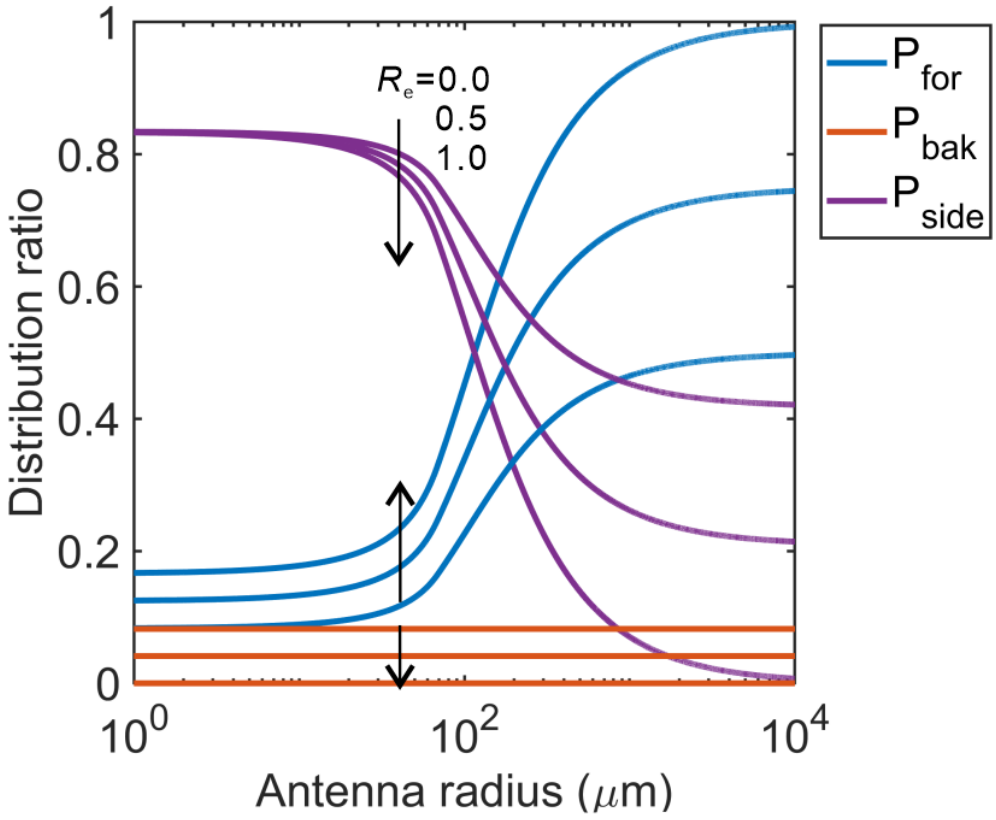

Figure S 7: P_{for}, P_{bak}, and P_{side} of the nanoantenna phosphor with T_p = 105 μm with varied R_a and different R_e of 0.0, 0.5 and 1.0.

5 Design and performance of DBR

The DBR was designed to transmit the excitation blue light (λ= 460 nm) and reflect the yellow PL. We focused on a two-layer DBR of SiO_2 and TiO_2 to minimize the experimental difficulties. We calculated the performance of the designed system, SiO_2 (90 nm) and TiO_2(180 nm) on YAG:Ce (infinite thickness) by transfer matrix, as depicted in Fig. S8(a). Because the DBR is only two-layers, the performance was not very high; the reflectance of the PL was around 40%.

We measured the transmittance of the fabricated DBR on a flat YAG:Ce (T_p= 325 μm) (see Fig. S8(b)). The agreement between the experimental and calculated transmittance indicates that the fabrication was done as designed. The performance depends on the angle of incidence, and thus the effect of the DBR was reproduced with the reflectivity 0f 0.15, which is lower than the calculated value of 0.4 (see Sec. 2.4 in the main text).

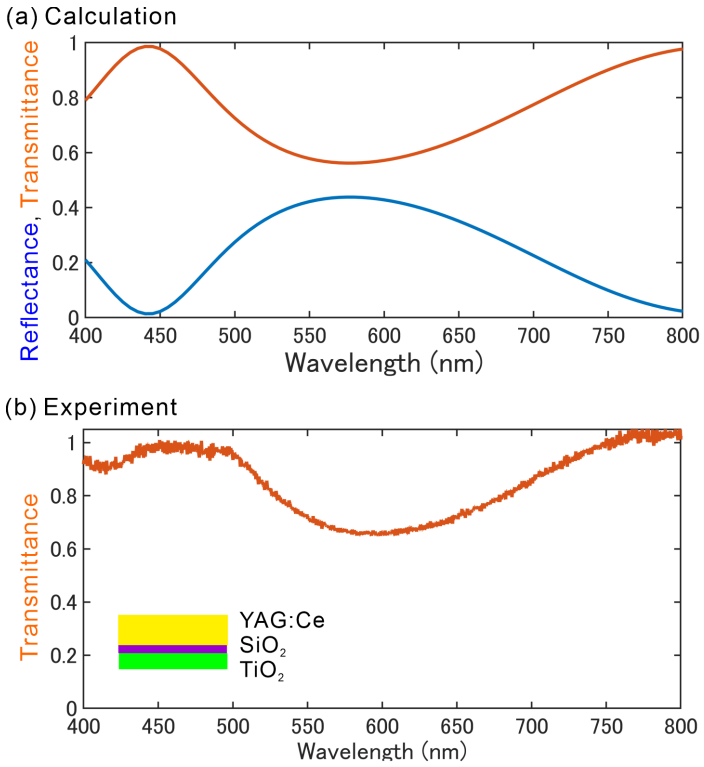

Figure S 8: (a) Specular reflectance and transmittance at normal incidence of the DBR calculated by transfer matrix. (b) Specular transmittance at normal incidence measured for the DBR on a flat YAG:Ce substrate. The inset sketches the sample.

References

(1) Sun, H.; Piquette, A.; Raukas, M.; Moustakas, T. Enhancement of Yellow Light Extraction Efficiency of $Y_3Al_5O_{12}$:Ce^{3+} Ceramic Converters Using a 2-D TiO_2 Hexagonal-Lattice Nanocylinder Photonic Crystal Layer. *IEEE Photonics J.* **2016**, *8*, 1–10.

(2) Gorsky, S.; Zhang, R.; Gok, A.; Wang, R.; Kebede, K.; Lenef, A.; Raukas, M.; Negro, L. D. Directional light emission enhancement from LED-phosphor converters using dielectric Vogel spiral arrays. *APL Photon.* **2018**, *3*, 126103.

(3) Gorsky, S.; Britton, W. A.; Chen, Y.; Montaner, J.; Lenef, A.; Raukas, M.; Negro, L. D. Engineered hyperuniformity for directional light extraction. *APL Photon.* **2019**, *4*, 110801.

(4) Mao, A.; Karlicek, R. F. Surface patterning of nonscattering phosphors for light extraction. *Opt. Lett.* **2013**, *38*, 2796–2799.

(5) Kamakura, R.; Murai, S.; Yokobayashi, Y.; Takashima, K.; Kuramoto, M.; Fujita, K.; Tanaka, K. Enhanced photoluminescence and directional white-light generation by plasmonic array. *J. Appl. Phys.* **2018**, *124*, 213105.

(6) de Mello, J. C.; Wittmann, H. F.; Friend, R. H. An improved experimental determination of external photoluminescence quantum efficiency. *Adv. Mater.* **1997**, *9*, 230–232.